Morphological and Crystallographic Controls of Replacement of Calcite and Aragonite by Cerussite and Otavite

YoungJae Kim[1], Aniket Tekawade[2], Sang Soo Lee[1], and Paul Fenter[1,*]

[1]Chemical Sciences and Engineering Division, Argonne National Laboratory, Lemont, IL, USA

[2]Data Science and Learning Division, Argonne National Laboratory, Lemont, IL, USA

* Corresponding author: E-mail: fenter@anl.gov

Abstract

Mineral replacement reactions are essential solid-fluid interactions in natural and industrial processes including metasomatism, diagenesis, and metamorphism, and sequestration of metal toxins from polluted water. Here, we explore the morphological evolution of aragonite and calcite (polymorphs of $CaCO_3$) during their replacement by cerussite ($PbCO_3$, an isomorph of aragonite) and otavite ($CdCO_3$, an isomorph of calcite) in acidic aqueous solutions (with initial pH 3 to 4). Observations using scanning electron and synchrotron-based transmission X-ray microscopies reveal the formation of pseudomorphic shells (~5 to 10 μm thick) of cerussite and otavite when Pb^{2+} is reacted with either calcite or aragonite and when Cd^{2+} is reacted with aragonite. The formation of pore space at the substrate-precipitate interface and within the precipitate is found to be key in promoting chemical exchange between the dissolving phase and the solution. In contrast, minimal reactivity is observed when Cd^{2+} is reacted with calcite. These results demonstrate that the lack of substrate-precipitate epitaxy (either because of inconsistent symmetries or due to large lattice constant mismatch) is a critical factor that enables replacement of primary $CaCO_3$ minerals by Pb- or Cd-bearing secondary minerals while the presence of epitaxial relationships inhibit those reactions. When calcite and aragonite coexist, the replacement of aragonite by cerussite and otavite occurs preferentially over calcite. We postulate that the relative reactivity of calcite and aragonite to Pb^{2+} and Cd^{2+} can be determined by interplay between morphological and crystallographic properties of $CaCO_3$ materials as well as solution chemistry. Our results demonstrate that

coupled dissolution-precipitation processes of carbonate minerals play an important role in controlling mobility and bioavailability of lead and cadmium in environments where acidic metal-contaminated water interacts with carbonate-rich rocks and soils.

Keywords: mineral replacement, calcite, aragonite, cerussite, otavite, transmission X-ray microscopy

1. Introduction

Calcite and aragonite are the two most common polymorphs of calcium carbonate minerals ($CaCO_3$) in nature. Calcite is the most stable form of $CaCO_3$ under ambient conditions while aragonite is the high-pressure polymorph of $CaCO_3$. Both calcite and aragonite commonly form as a main constituent in coral reefs and shells in marine environments (Checa et al., 2007; Gillikin et al., 2005; Keith et al., 1964). Because their mineral-water interfaces are highly reactive to dissolved ions, calcite and aragonite play an important role in controlling the fate of various metal ions, in natural and engineered settings, through processes including adsorption, incorporation, and precipitation (Callagon et al., 2014; Davis et al., 1987; Elzinga et al., 2006; Kang et al., 2014; Rouff et al., 2004; Sturchio et al., 1997; Zavarin et al., 2005).

Mineral replacement reactions can occur via a coupled dissolution-precipitation process in which a substrate phase dissolves in contact with fluid and is replaced by a more stable precipitate. These reactions are essential in many natural and industrial processes including chemical weathering, metasomatism, diagenesis, metamorphism, and sequestration of metal toxins from polluted water (Putnis, 2002, 2009; Ruiz-Agudo et al., 2014). A key feature of a mineral replacement reaction is the preservation of the original dimensions of the substrate phase (i.e., pseudomorphism). The shape preservation indicates that the reaction front migrates from the external surfaces of the original mineral into the interior of the substrate crystal. The structure, composition, and morphology of the replaced crystal are known to be controlled by various factors including the difference in solubility between the substrate and the

precipitate, the relative rates of the dissolution and precipitation reactions (Putnis, 2002, 2009; Ruiz-Agudo et al., 2014), and the development of porosity in the precipitating phase that promotes chemical exchange between the dissolving phase and the solution.

Replacement reactions typically occur under far-from-equilibrium conditions that maintain sustained disequilibria in which the reactant solid phase remains undersaturated while the product solid phase becomes supersaturated. These conditions can dramatically influence reaction mechanisms and pathways in elemental transport under geochemically relevant conditions. For example, the highly acidic fluids in acid mine drainage sites contain large amounts of heavy metal ions (e.g., Pb^{2+}, Hg^{2+}, Cd^{2+}) (Li et al., 2009), which can react with carbonate minerals that commonly exist in mine tailings as well as contaminated soils and sediments. The pseudomorphic replacement of sparingly-soluble $CaCO_3$ minerals by less-soluble secondary minerals containing these metals (e.g., $CaCO_3 + Pb^{2+} \rightarrow PbCO_3 + Ca^{2+}$) can inhibit the geochemical transport and biological availability of these metal toxins (Abdilla et al., 2022; Yuan et al., 2016). The same mechanism may also be relevant to geomechanical phenomena, such as the sequestration of CO_2 through the coupled dissolution of mafic silicate minerals in CO_2-saturated injection waters and precipitation of carbonate minerals (e.g., CarbFix). As such, understanding the controls over the reactivity of carbonate minerals under conditions of disequilibria (e.g., acidic pH) is broadly important. The current study focuses on the reactivity of calcite and aragonite in acidic pH solutions in the presence of two common toxic metal ions: Pb^{2+} and Cd^{2+}. Both of these metals are constituent elements of relatively insoluble carbonate minerals, but their different crystal structures allow the crystallographic controls over these reactions to be isolated. Furthermore, the facile reactivity of carbonate minerals at ambient conditions makes them well suited for systematic measurements to identify the relevant chemical and crystallographic controls over these reactions.

Systematic investigations on the interfacial reactivity of calcite and aragonite in acidic metal-rich fluids have been reported recently. For example, in acidic Pb^{2+} containing solutions, replacement of calcite and aragonite by cerussite ($PbCO_3$) can proceed through coupled dissolution-precipitation

processes, while maintaining the overall carbonate grain morphology (Kim et al., 2021; Yuan et al., 2018; Yuan et al., 2016). This combination drives dissolution of calcite and aragonite (having solubility products, $K_{sp} = a_{Ca^{2+}} \cdot a_{CO_3^{2-}} = 10^{-8.48}$ and $10^{-8.34}$, respectively, where a represents the ion activity at equilibrium; Plummer and Busenberg (1982)) followed by precipitation of cerussite having a significantly lower solubility (i.e., $K_{sp} = a_{Pb^{2+}} \cdot a_{CO_3^{2-}} = 10^{-13.76}$; Xiong (2015)). It is proposed that the growth rates and modes of cerussite on dissolving calcite and aragonite can be controlled by spatial distribution of solution pH and ion concentrations, which determine the (local) saturation index of the precipitate (Kim et al., 2021; Yuan et al., 2016). In addition, previous studies have compared Pb uptake by calcite *vs.* aragonite in replacement reactions that form cerussite as the final product (Di Lorenzo et al., 2019; Gamsjäger et al., 1984; Godelitsas et al., 2003; Kim et al., 2021; Miyake et al., 1988). However, there are some significant discrepancies among these studies. Gamsjäger et al. (1984) reported batch experiment results showing that Pb^{2+} uptake by aragonite occurs to greater extents and at faster rates than that by calcite. In contrast, observations made by Di Lorenzo et al. (2019) revealed a lower reactivity of aragonite to Pb^{2+} compared to that of calcite, from batch experiment combined with scanning electron microscopy (SEM), and suggested that the surface passivation of aragonite by cerussite could occur because the precipitate and substrate phases are isostructural (orthorhombic, 2/m2/m2/m). Our previous observations indicated that the relative reactivity of calcite and aragonite in acidic Pb^{2+} containing solution may be determined by morphological features of these polymorphs, which control the local saturation index of cerussite near the $CaCO_3$ substrate (Kim et al., 2021). In turn, these previous studies highlight the need for a systematic investigation of various factors that control the reactivity of calcium carbonate polymorphs with heavy metals in acidic aqueous solutions.

Similar considerations can be applied to the reaction of calcium carbonate with acidic solutions containing Cd^{2+}. Since otavite ($CdCO_3$) has a lower solubility ($K_{sp} = a_{Cd^{2+}} \cdot a_{CO_3^{2-}} = 10^{-12.24}$; Rai et al. (1991)) than calcite and aragonite, it is expected that its growth can be induced by dissolution of $CaCO_3$ in acidic Cd^{2+} containing solutions, in analogy to what is observed with Pb^{2+}. One important difference

when otavite grows on a calcite substrate, however, is the close structural match between otavite and calcite. Otavite has the same crystal structure as calcite (trigonal, $\bar{3}2/m$) with only a small lattice misfit to the calcite lattice spacing (ranging from 1 to 3 % with respect to the surface lattice spacings in the calcite and otavite (104) planes). Consequently, otavite can be expected to grow as a continuous epitaxial film that is coherently strained to the calcite substrate. Growth of a continuous film may inhibit the progress of the coupled dissolution-precipitation reactions (Pérez-Garrido et al., 2007; Prieto et al., 2003; Xu et al., 2014) that require the dissolution of the substrate as a source of carbonate ions.

Relevant to the understanding of replacement reactions of calcite by otavite are previous observations of otavite growth on calcite in otavite-supersaturated solutions. Atomic force microscopy (AFM) and synchrotron X-ray reflectivity (XR) studies have demonstrated that otavite films grow as coherently strained films on the calcite (104) plane, consistent with the expectation from the crystallographic similarity between two solid phases (Chiarello and Sturchio, 1994; Chiarello et al., 1997; Pérez-Garrido et al., 2007; Xu et al., 2014). The thickness of these otavite films ranged from a few to tens of nm depending on the initial saturation index of the reacting solution with respect to otavite. When grown from solutions that were supersaturated with respect to otavite, it was found that the otavite film morphology evolved as would be expected for an epitaxially strained layer, including the growth of a coherently strained otavite film for thicknesses below the critical thickness (e.g., 3 and 15 nm for the calcite and dolomite (104) surfaces, respectively), followed by the development of a strain-relieved film (presumably due to a combination of dislocations and the development of a morphologically rough film) (Callagon et al., 2017; Chiarello and Sturchio, 1994; Chiarello et al., 1997; La Plante et al., 2018).

Significantly less is known about the reaction mechanisms of aragonite with dissolved Cd^{2+} than those of calcite with dissolved Cd^{2+}. Prieto et al. (2003) reported a significantly higher Cd uptake by aragonite from aqueous $CdCl_2$ solutions compared to that by calcite. Cubillas et al. (2005) found that in the presence of dissolved Cd^{2+}, the dissolution rates of calcite were lower than that of aragonite, which induced a greater extent of Cd precipitation by aragonite than calcite. In both studies, the differences in

Cd sorption were attributed to different growth modes of otavite on the substrate minerals. These findings from previous studies were mainly based on batch sorption experiments combined with microscopic observations made using SEM to contrast the final product of otavite grown on aragonite with no discrete otavite crystals found on the calcite surface. As demonstrated from our previous study (Kim et al., 2021), SEM is useful in visualizing external morphologies of the product phase upon mineral replacement but does not provide direct insights into the product-substrate interfaces. Although there is some consensus that Cd uptake by aragonite can occur via mineral replacement (i.e., similar to Pb uptake by calcite and aragonite), this insight has not yet been supported by direction observations of the morphological relationships between the host phase and the secondary mineral.

Here, we explore the morphological evolution of calcite and aragonite prepared in three different forms (i.e., single crystals, crushed minerals, and mixed crystals) during reaction with dissolved Pb^{2+} or Cd^{2+} to understand the morphological and crystallographic controls over the replacement of calcium carbonate polymorphs by cerussite and otavite. In these measurements, the reactivity of these calcium carbonate polymorphs is observed in acidic conditions (initial pH = 2.7 to 4.0) that maintain a continued undersaturation of the calcium carbonate substrate while the product phase nucleates and grows, thereby ensuring a sustained disequilibrium. A unique aspect of our approach is that we compare the different reaction modes leading to the formation of cerussite and otavite by combining observations of changes to the *external* morphology of calcite and aragonite by SEM with parallel observations of the *internal* structure of replaced calcite and aragonite crystals using synchrotron transmission X-ray microscopy (TXM). As demonstrated in our previous studies (Kim et al., 2021; Yuan et al., 2016), TXM imaging enables direct observations of the product-substrate interface formed during mineral replacement.

This approach has led to multiple new insights into the reaction process. For example, TXM images of aragonite replaced by otavite are the first to provide direct evidence that this replacement reaction is enabled by reactant (Cd^{2+}) transport through pore spaces within the otavite product and between the otavite and aragonite phases. These morphological and chemical observations also reveal that the

outcomes of these replacement reactions (including dissolution and growth rates and patterns) depend on the crystal structure and initial morphologies of calcium carbonate polymorphs. This suite of measurements allows us to make direct comparisons of four reaction systems having host minerals and reaction products with either the same or different crystal symmetry groups (i.e., minerals having the calcite and aragonite crystal structures, respectively) and to explore the role of lattice strain when they are isostructural (i.e., small lattice mismatch between calcite and otavite vs. the large lattice mismatch between aragonite and cerussite). The results show that the lack of epitaxial relationships between the reactant and the product (either due to different crystal symmetry groups, for calcite–cerussite or otavite–aragonite, or due to significant lattice mismatch for isostructural minerals, for aragonite–cerussite) is a critical factor that enables mineral replacement reactions to penetrate into the substrate phase, while the presence of true epitaxial relationship inhibits those reactions (e.g., for calcite–otavite). Our results also show how the interfacial reactivity of calcite and aragonite with Pb^{2+} and Cd^{2+} is influenced by the dissolution rate of calcium carbonate. These results are compared with previous observations of mineral replacement reactions.

2. METHODS

Synopsis of experiment

Calcite and aragonite have moderate solubilities and distinct crystal structures (trigonal and orthorhombic, respectively). We reacted calcite and aragonite crystals in acidic Pb^{2+} and Cd^{2+} aqueous solutions to induce replacement of these polymorphs by $PbCO_3$ (cerussite, an isomorph of aragonite) and $CdCO_3$ (otavite, an isomorph of calcite), which are much less soluble in water than the $CaCO_3$ polymorphs. The initial solutions (at the initial pH of 2.7–4.0) were undersaturated with respect to both the $CaCO_3$ minerals and the secondary phases. The growth of the new phase, if observed, was initiated at the $CaCO_3$-water interface where the local concentration of carbonate was sufficiently high to induce the precipitation of cerussite and aragonite. All observations were made at room temperature.

The four replacement reactions (i.e., the combination of two mineral substrates, calcite and aragonite, and two metal ions, Pb^{2+} and Cd^{2+}) represent transformations between the dissolving and precipitating phases with the same or distinct crystal structures, and with large vs. small lattice constant differences for isostructural phases (i.e., aragonite by cerussite and calcite by otavite, respectively). The lattice spacing differences between aragonite and cerussite are 4–7 % (with respect to the aragonite (001), (010), and (110) planes; Supporting materials) and those between calcite and otavite are 1–3 % (with respect to the calcite (104) plane), respectively. In comparison, the replacement of calcite by cerussite, and aragonite by otavite, involves phases with distinct crystal structures. Therefore, comparing morphological characteristics of these four replacement reactions offers direct insights into how the mineral replacement reactions are controlled by crystallographic relationship and lattice mismatch between the substrates and precipitates.

Minerals and reagents

Calcium carbonate polymorphs were prepared in three different ways. 1) Individual crystals of calcite and aragonite were co-grown on Kapton films using the ammonium diffusion method (Hu et al., 2012; Ihli et al., 2013). 2) Aggregates of calcite and aragonite were prepared by mixing carbonate- and calcium-containing solutions at 70 ℃ (Wray and Daniels, 1957) . 3) Powder specimens of calcium carbonate were prepared by crushing and sieving natural calcium carbonate minerals, i.e., calcite (Chihuahua, Mexico) and aragonite (Ivanpah Mt., California, USA), to obtain particles in size ranging from 47 to 53 μm (similar to the crystals grown by the ammonium diffusion method). These prepared $CaCO_3$ samples were reacted with acidic Pb^{2+}- or Cd^{2+}-containing solutions. Pb(II) and Cd(II) stock solutions were prepared using Milli-Q® water (resistivity ≥ 18.2 MΩ·cm; TOC < 5ppb), lead nitrate ($Pb(NO_3)_2$, Sigma Aldrich; purity of ≥ 99 %), and cadmium chloride hemipentahydrate ($CdCl_2 \cdot 2½H_2O$, Mallinckrodt; purity of 99-100 %).

Reaction protocols

Mineral replacement reactions for individual crystals, aggregates, and powder specimen of calcite and aragonite were performed in a fluid cell containing $CaCO_3$ crystals in contact with a static solution with 1−5 mM Pb(II)/1−10 mM Cd(II), an initial pH of 2.7–4.0, and a solid mass to solution volume ratio of 0.1–0.37 g/L. As calcite and aragonite were undersaturated in this initial solution, the dissolution of $CaCO_3$ minerals occurred at increasing solution pH and (bi)carbonate concentrations. We focused on conditions and reaction times where the $CaCO_3$ phases remain undersaturated throughout the reaction period.

For reaction of aragonite with Pb^{2+} and Cd^{2+} and calcite with Pb^{2+}, the final Pb- and Cd-containing solutions, after reaction for 16 to 24 h, displayed the pH ranging from 4.2 to 4.8 and from 5.5 to 6.0, respectively, with total dissolved carbonate concentrations of 1–4 mM. The saturation index (SI) of cerussite ranged from −1.2 to 0.5 and that of otavite from 0.6 to 2.1. These indicate that the solution chemistry evolved as the dissolution of the $CaCO_3$ phase continued during reaction, from undersaturation with respect to cerussite and otavite to supersaturation with respect to both of these phases during the reaction. A different behavior is observed for reactions of calcite with Cd^{2+}: the final solution pH was 5.5 to 6.0 and the total dissolved carbonate concentration was only 20 μM. This low carbonate concentration suggests the inhibited dissolution of calcite. The SI of otavite in the final solution ranged from −1.2 to 0.0, indicating that the solution was undersaturated or in equilibrium with respect to otavite.

After the desired reaction time, the samples were gently rinsed with ethanol and air-dried. These reacted $CaCO_3$ samples were imaged using a Phenom scanning electron microscope (SEM) with energy dispersive X-ray spectroscopy (EDS) (Thermo Fisher Scientific) and transmission X-ray microscopy (TXM). The secondary phases were identified using X-ray diffraction (XRD).

Transmission X-ray Microscopy (TXM)

Synchrotron X-ray nano-tomography measurements were performed at beamline 32-ID-C at the Advanced Photon Source (APS) in Argonne National Laboratory (ANL). The incident X-ray photon

energy was 8 keV and a field of view of 51 × 51 μm^2 was used. The sample was imaged in 721 projection directions within a rotation angle of 180°. The exposure time was 0.5 to 1 s per image and the spatial resolution of the image was 49 nm. The projection data was reconstructed using Tomopy (De Carlo et al., 2014; Gürsoy et al., 2014; Pelt et al., 2016). The acquired images were further processed using an open-source 3D image segmentation code, CTSegNet developed by Tekawade et al. (2021) that uses deep learning to automate the classification of pixels into specific phases (e.g., background, cerussite/otavite, and calcite/aragonite). CTSegNet applies multiple passes of an encoder-decoder 2D convolutional neural network (CNN) onto orthogonal axes of a 3D reconstructed grayscale volume to produce an ensemble voted mask that captures 3D information about pixel intensity variation in the different phases. The segmented images were analyzed and visualized using 3DSlicer (www.slicer.org; Fedorov et al. (2012)) and Paraview (Ayachit, 2015).

X-ray diffraction (XRD)

Silicon "zero-background" sample holders (MTI corporation; www.mtixtl.com) were used for XRD. Samples were transferred to the holders in a form of isopropyl alcohol slurry and then dried in air for 30-60 min. XRD patterns were obtained using a Bruker D8 Advance diffractometer with a step size of 0.008° 2θ. Cu Kα radiation (λ = 0.15418 nm) was used and the measurement time was 1 s per step.

3. RESULTS

3.1. Replacement reactions of calcite and aragonite in acidic Pb^{2+} and Cd^{2+} solutions

Powder specimens of calcium carbonate polymorphs before and after reaction in acidic Pb^{2+}- or Cd^{2+}-containing solutions (initial pH = 2.7; 5 mM $[Pb^{2+}]_{initial}$ or 5 mM $[Cd^{2+}]_{initial}$, respectively) for 16 hr were examined using XRD and SEM. The XRD measurement confirms that the mineral specimens used for the replacement reactions consisted of calcite and aragonite, respectively (Fig. 1) without any evidence for secondary phases. Cerussite was identified as the main product of reaction of calcite and aragonite with acidic Pb^{2+}-containing solution (Fig. 1). The rod-shaped cerussite crystals grown on both calcite and

aragonite were observed by SEM (Fig. 2 A and B). The formation of cerussite is consistent with previous studies of calcium carbonate mineral evolution in the presence of dissolved Pb^{2+} (Di Lorenzo et al., 2019; Gamsjäger et al., 1984; Yuan et al., 2018; Yuan et al., 2016).

The main product from the reaction of aragonite with acidic Cd^{2+}-containing solution was Cd-rich $Cd_xCa_{(1-x)}CO_3$ solid solution (hereafter referred to as otavite) (Fig. 1A). The otavite crystals that formed on aragonite were sub micrometers to few micrometers in size and rhombohedral in shape (Fig. 2C). Unlike the other three reaction systems, in reaction of calcite with Cd^{2+}, no discrete secondary particles were observed by SEM (Fig. 2D) nor identified by XRD (Fig. 1B). We did, however, detect very small EDS signals from Cd^{2+} on the calcite grains, corresponding to 0.03 to 0.11 at.% (Fig. S.1) suggesting that an interface-limited reaction may occur on these surfaces. Since EDS is not a surface-specific technique, the Cd content of surface precipitates, if formed, might be higher than this concentration range.

3.2 Morphological evolution during mineral replacement

Morphological changes of calcite, aragonite, and calcite/aragonite mixture during replacement reaction in acidic Pb- and Cd-containing solutions were imaged using SEM (Fig. 3). Before the reaction, the aragonite starting material occurred in aggregates less than 150 μm in size but with spiky morphologies (Fig. 3A and C). Pristine calcite starting material was grown as individual euhedral crystals, 30 to 80 μm in size (Fig. 3B and D).

The surfaces of aragonite crystals reacted in 1 mM $[Pb^{2+}]_{initial}$ solution at pH 3.0 are gradually covered by cerussite, which appears as bright phases in the SEM images (Fig. 3A). While this morphological change occurred within the first hour (Fig. 3A), aragonite crystals barely changed in size and external morphology after additional reaction times (Fig. S.2). Calcite crystals reacted in a solution having the same solution composition decreased in size throughout the reaction and developed spatially modulated surface morphologies (Fig. 3B), due to the dissolution of the calcite surface in the presence of dissolved

Pb^{2+} (Yuan et al., 2018). After 6 hr of reaction, the formation of cerussite was observed near the contact of the calcite crystal on the Kapton support similar to the observations in the previous study (Yuan et al., 2018; Yuan et al., 2016). This behavior can be contrasted with that occurring in Cd-containing solutions. In a solution with 10 mM $[Cd]_{initial}$ at pH 4.0, the precipitation of otavite on the aragonite substrate gradually proceeded within first 3 hr (Fig. 3C) and there were little changes in size and external morphology afterward (Fig. S.2), leading to reacted structures that appeared morphologically similar to that observed in Pb-containing solutions. In contrast to this, calcite crystals reacted with the same Cd-containing solution showed minimal changes after reaction for 12 hr (Fig. 3D) and no evidence of the formation of otavite as a discrete phase. These results showed that the growth process of cerussite on dissolving aragonite was generally similar to that of otavite on aragonite, but that the growth of cerussite was significantly faster. The behavior of calcite was distinct from aragonite. The presence of Pb^{2+} altered the dissolution process of calcite (Yuan et al., 2019), and the nucleation of cerussite on calcite occurred at slower rates than that on aragonite. In contrast, the present of Cd^{2+} appeared to inhibit or slow the dissolution of calcite under these conditions.

Aragonite/calcite mixtures were reacted with Pb^{2+} and Cd^{2+} to further examine relative reactivities of these calcium carbonate polymorphs with dissolved lead and cadmium ions (Fig. 4). In these mixtures, aragonite had a rod-shaped morphology, which indicates that these crystals grew along the c-axis of the aragonite structure (Wang and Han, 2014; Zeng et al., 2018). In acidic Pb^{2+} containing solution, replacement by cerussite began at the tips of aragonite crystals and gradually proceeded over the body of these crystals for the first 2 hr. In some cases, the core aragonite was fully dissolved, leaving pseudomorphic shells of cerussite after reaction for 4 hr (Fig. 4A). During this morphological evolution, cerussite replacing aragonite crystals grew dominantly along the c-axis of the substrate structure (Fig. 4). In reaction with dissolved Cd^{2+}, sub-micrometer-sized otavite crystals grew on rod-shaped aragonite crystals, covering the entire aragonite surfaces within the first 4 hr. In the same acidic Pb- and Cd-containing solutions, calcite showed rounded edges by dissolution but replacement by lead and cadmium

carbonate was rare (Fig. 4). Overall, these results show that precipitation of cerussite and otavite preferentially occurred on aragonite over calcite when aragonite and calcite coexist.

3.3 pH evolution during mineral replacement.

The nature of these replacement reactions was further constrained by the solution chemistry monitored as the reaction progressed. To this end, the solution pH was measured as a function of time during reaction of calcite and aragonite powder with dilute hydrochloric acid (at initial pH = 2.7) in the absence and presence of Pb^{2+} or Cd^{2+} (5 mM $[Pb^{2+}]_{initial}$ or 5 mM $[Cd^{2+}]_{initial}$, respectively) (Fig. S.3). In the Pb^{2+}- and Cd^{2+}-free systems, the solution pH increased with time up to 7.6 after 24 hr. This increasing pH is expected from the dissolution as,

$$CaCO_3(s) + H^+ = Ca^{2+} + HCO_3^- \quad (1)$$

When calcite and aragonite were reacted with solutions containing Pb^{2+}, the pH stabilized after 10 min of reaction at 4.6 to 4.8. We postulate that this observation reflects a balance between $CaCO_3$ dissolution (Eq. 1) and $PbCO_3$ precipitation as

$$Pb^{2+} + HCO_3^- = PbCO_3(s) + H^+ \quad (2)$$

In reaction of aragonite with Cd^{2+}-containing solution, pH increased to 6.4 during the first 1 hr, followed by a gradual decrease down to pH 6.0 after 24 hr of reaction. The initial increase is consistent with those observed in the Cd^{2+}-free solution while the subsequent decrease likely reflects the delayed onset of otavite precipitation. When calcite was reacted with Cd^{2+}, pH increased from 2.7 to 5.2 during the first 10 min, followed by a gradual increase to 5.7 until 24 hr. Notably, the initial increase was slower than that in Cd^{2+}-free solution. While this behavior appears qualitatively similar to that for Pb reacting with calcite and aragonite (where replacement reactions occur readily), the lack of any significant replacement reactions in the Cd/calcite systems (i.e., with no calcite dissolution observed by SEM (Fig. 3D) and no otavite precipitation identified by XRD (Fig. 1B)) indicates that the slow pH evolution is due to the inhibited reactivity at the calcite surfaces. That is, interactions of Cd with the reactive sites of

calcite (e.g., via sorption on step and kink sites or the formation of a continuous film, see Section 4.1 for detailed discussion) passivate the surfaces, resulting in a decrease in dissolution rate and limited replacement of calcite by otavite.

3.4 Internal structures of replaced crystals of calcite and aragonite

The internal structures of $CaCO_3$ minerals after the reaction with acidic Pb- and Cd-containing solutions were examined using TXM (Fig. 5). In these TXM images, the brightness indicates the density of the materials such that lead and cadmium carbonate appear brightest, while calcium carbonate has intermediate contrast, and air is the darkest. These phases consisting of reacted $CaCO_3$ minerals were segmented and visualized in three dimensions (Fig. 6). Replacement of aragonite and calcite by cerussite began at the external surfaces of the crystals and propagated inward (Fig. 5 A and B). The cerussite layers on these substrates were typically ~5 to 10 μm thick. Otavite initially nucleated on the external surface of aragonite. Replacement of aragonite by otavite resulted in similar morphologies with the formation of a thick product and the presence of pores between the otavite and aragonite phases (Figs. 5D). In contrast, Cd-reacted calcite crystals remained visually unchanged (Fig. 5E), which indicates that the formation of otavite either did not occur or was limited to a thin layer on the external surface of calcite. In aragonite/calcite mixtures reacted with Pb^{2+} and Cd^{2+}, the cerussite and otavite layers on the aragonite substrate were sub micrometers to few micrometers thick (Fig. 5C and F).

These segmented images of the internal structure of the reacted $CaCO_3$ minerals provide direct evidence for the important role of porosity in the replacement reactions. Specifically, we observe pores separating the reactant and the product phases for all cases in which a replacement reaction was observed in process (i.e., with both reactant and product phases present). For example, pores are ~100 nm wide at the boundaries between the cerussite precipitate and the $CaCO_3$ substrate (Fig. 5A to C; Fig. 6A and B), consistent with a previous study (Kim et al., 2021; Yuan et al., 2016). Similar pores were observed between otavite and aragonite phases (Figs. 5F and CD). Additional pores developed within the precipitate phases, most notably for cerussite on dissolving calcite (Fig. 6A). These pore spaces can act as

fluid channels during the reactions, facilitating chemical exchange between the substrate and bulk solution.

4. DISCUSSION

4.1. Formation of porosity upon the mineral replacement of calcite and aragonite

Our SEM and TXM imaging results (Fig. 2 to 5) show similarities and differences among structural outcomes from the four replacement reactions under the equivalent conditions in terms of initial pH and metal concentrations. Under the disequilibrium conditions of the present study (mainly driven by acidic pH), pseudomorphic replacement by cerussite (an isomorph of aragonite) and otavite (an isomorph of calcite) were observed when calcite and aragonite were reacted with Pb^{2+} and aragonite with Cd^{2+} (Figs. 2 to 4). One key feature found in these pseudomorphic replacement reactions was the formation of pores between the substrate and precipitate (~ 100 nm in thickness) (Figs. 5 and 6). Through these pores, chemical exchange is facilitated between the dissolving $CaCO_3$ mineral, the precipitating cerussite/otavite, and the bulk solution. The development of porosity plays a key role in promoting the advancement of a reaction front from the mineral-water interface to the internal structure of a crystal. In turn, these morphological features (both external and internal ones) observed in replaced $CaCO_3$ crystals define the reaction mechanisms addressed in this study as pseudomorphic replacement (which satisfies the definition described in Putnis (2009)). Here, we propose a conceptual model to demonstrate how the formation of porosity upon the mineral replacement of calcium carbonate can be controlled by the crystallographic relationship between the dissolving and the precipitating minerals and the differences in the molar volumes of these solid phases.

We conclude that the growth mode of the precipitate is a critical factor in controlling the development of porosity upon mineral replacement. Otavite has the same crystal structure as calcite (trigonal, $\bar{3}2/m$) with small lattice spacing misfit with respect to the calcite (1 to 3 % with respect to the lattice spacing of the calcite and otavite (104) planes). Previous studies have observed the epitaxial growth of otavite on

calcite with epitaxy mainly due to the crystallographic matching between otavite and calcite (Chiarello and Sturchio, 1994; Chiarello et al., 1997; La Plante et al., 2018; Pérez-Garrido et al., 2007; Xu et al., 2014). It has been postulated that these epitaxial layers may prevent calcite from further dissolution and thus stop the coupled dissolution-precipitation (Pérez-Garrido et al., 2007; Prieto et al., 2003; Xu et al., 2014).

The important role of epitaxy in inhibiting a replacement reaction is highlighted by comparing the extended replacement of aragonite with Pb^{2+} to the limited reaction of calcite with Cd^{2+} under equivalent conditions (Figure 2 to 5). Although cerussite and aragonite also have the same crystal structure, there is a larger lattice misfit between these two minerals, ranging from 4 to 7%. These differences can be characterized through the estimation of the "critical thickness" of the precipitating phase (La Plante et al., 2018; Matthews and Blakeslee, 1974), corresponding to the maximum thickness of an epitaxially registered film that can form before the development of dislocations (see Supporting materials for details). Ultimately, this estimation provides a way to evaluate the structural relationships that the precipitate can maintain with the substrate and the expected growth mode. The estimated critical thickness for otavite on calcite is ~3 nm, indicating that it can be physically stable as a continuous film up to that thickness. In contrast, the critical thickness for cerussite on aragonite is ~0 nm, indicating that continuous cerussite films onaragonite interface are not stable. This might suggests, for example, that the initial cerussite product would tend to grow as isolated islands to minimize contact between cerussite and aragonite. As a result, a portion of the aragonite surface will remain uncoated and exposed to solution during these reactions, which will allow the replacement reaction to continue. This calculation is fully consistent with the observations of pores at the cerussite/aragonite interface as seen in our previous (Kim et al., 2021) and present studies. In contrast, the larger critical thickness of otavite coatings on calcite, which enables a continuous film to form up to thicknesses of ~10 molecular-layers, implies that the calcite surface will not be exposed to solution after an initial reaction period. This would significantly

inhibit the transport of reactants to and from the interface since it would be necessary to occur through solid-state diffusion rather than dissolution/precipitation at the mineral-aqueous solution interface.

Among the substrate-precipitate crystallographic relationships examined in this study, replacement of calcite by cerussite and of aragonite by otavite are ones in which the substrate and precipitate phases have distinct crystal structures. Our TXM image data of these two replacement reactions reveal that the substrate surfaces do not become fully passivated by the growth of the precipitates (Figure 5 and 6). We postulate that the incomplete passivation by precipitates is mainly due to their structural inconsistencies with the substrate. Initially, cerussite and otavite can nucleate, as discrete phases, on the substrate when fresh aragonite crystals are reacted in acidic Cd^{2+}- and Pb^{2+}-containing solution and when fresh calcite crystals are reacted in acidic Pb^{2+}-containing solution (Fig. 3). These nuclei can eventually cover the external surface of the $CaCO_3$ substrate. But unlike the case for otavite on calcite, the structural heterogeneity of the precipitated layer (i.e., different shapes and orientations of distinct nuclei) enables reactant transport by solution through the pores and grain boundaries (Fig. 6). The chemical exchange is initiated at the mineral-water interface and continues throughout the reaction as the initial pore space at the interface evolves into internal gaps between the substrate and precipitate (Figs. 5 and 6).

Under our experimental conditions, we found no evidence for either the generation of porosity or the formation of otavite layers on the calcite substrate reacted with Cd^{2+}. In acidic Cd^{2+}-containing solution, calcite replacement by otavite can be limited by multiple processes at the calcite-water interface. Initially, the solution is undersaturated with respect to otavite and the dissolution of calcite becomes the source of carbonate in the solution. The dissolution rate of calcite would decrease upon Cd^{2+} adsorption on the surface (Cubillas et al., 2005; Hay et al., 2003; Pérez-Garrido et al., 2007). If the (local) saturation index of otavite becomes sufficiently high (e.g., through the dissolution of neighboring carbonate crystals), the nucleation of otavite could occur in the form of two-dimensional epitaxial layers or three-dimensional islands (Pérez-Garrido et al., 2007; Riechers and Kerisit, 2018; Xu et al., 2014) on top of a calcite surface.

But the formation of a continuous otavite layer on the calcite surface might be expected to significantly inhibit calcite dissolution, and therefore prevent further replacement reaction.

Upon the mineral dissolution-precipitation reaction, the difference in molar volume between the reactant and product is another key variable in controlling the formation of pores (Putnis, 2002, 2009). When the common elements or ions (e.g., carbonate in our case) are preserved, decrease in molar volume by the replacement reaction can cause the formation of pores within the solid phase. This is the case expected for replacement of calcite and aragonite by otavite: the molar volume of otavite ($V_{m,\ otavite}$ = 34.3 cm^3mol^{-1}) is smaller than those of calcite and aragonite ($V_{m,\ calcite}$ = 36.9 and $V_{m,\ aragonite}$ = 37.3 cm^3mol^{-1}). The molar volume of cerussite ($V_{m,\ cerussite}$ = 40.7 cm^3mol^{-1}) exceeds those of calcite and aragonite. Therefore, if all dissolved carbonate species are completely deposited into the cerussite product, the total volume of the solid phase would be increased as a result of the replacement reaction. During the dissolution-precipitation reaction in acidic Pb-containing solutions, however, the net carbonate loss from the substrate mineral by the reaction is equivalent to the sum of carbonate deposited in cerussite and carbonate dissolved in solution. In our experimental conditions, only part of carbonate ions dissolved from the substrate mineral is deposited into the precipitate mineral (this is most evident in the images in Fig. 3C, which show calcite crystals decreasing in size before the nucleation of $PbCO_3$). Therefore, our results indicate that the change in volume of the solid phase during the replacement is determined, at least in part, by the relative amount of the dissolving and precipitating phases and their molar volume ratio. In turn, the decrease in volume of the solid phase could contribute to the formation of pores upon the simultaneous dissolution-precipitation processes. Our considerations on the molar volumes of carbonate minerals are consistent with the concept that the formation of pore space upon mineral replacement is controlled by the relative amounts of the substrate and precipitate phases, which depend on their relative solubilities and the solid and fluid compositions (Putnis, 2002).

Our conceptual model described above demonstrates that the outcome of carbonate mineral replacement under highly acidic conditions is explained well by the substrate-precipitate structural

relationship and the differences in molar volume between the substrate and the precipitate. We expect that application of this model to carbonate replacement under different reaction conditions or to replacement of other substrate minerals may require consideration of the interplay between the parameters involved in this model as well as other factors that are not included in this model. For example, the surface passivation of host phases by non-isostructural product phases may occur when the reaction involves large positive molar volume change (Forjanes et al., 2020; Ruiz-Agudo et al., 2019). When replacement reactions involve significant volume changes, resulting stresses may induce generation of cracks in parent and product phases, which can act as reaction fronts in addition to pore space (Perdikouri et al., 2013; Xia et al., 2009).

4.2. Relative interfacial reactivities of calcite and aragonite to Pb^{2+} and Cd^{2+}

In this study, three different samples of $CaCO_3$ polymorphs were prepared and reacted with dissolved Pb^{2+} and Cd^{2+}. In the presence of Pb^{2+}, powder specimens of both calcite and aragonite underwent extensive replacement by cerussite (Figs. 1 and 2), while preferential replacement of aragonite over calcite occurred (with faster reaction rates) when individual $CaCO_3$ crystals and calcite/aragonite aggregates were reacted with Pb^{2+} (Figs. 3 and 4). We conclude that these differences in reactivity between calcite and aragonite with Pb^{2+} are largely determined by the morphological and crystallographic features of the $CaCO_3$ polymorphs under these conditions. Because the area-normalized dissolution rate constants of aragonite and calcite are approximately the same over the pH range examined in this study (initial pH = 2.7 to 4) (Busenberg et al., 1986), the rates would be largely controlled by their specific surface areas. Powder specimens of calcite and aragonite consist of particles with a similar range of size fraction (47 to 53 μm) and therefore, likely had comparable specific surface areas. In samples of individual $CaCO_3$ crystals and calcite/aragonite aggregates (Figs. 3 and 4), aragonite was of polycrystalline aggregates and bundles of rod-shaped crystals, respectively, and therefore likely had a larger surface area than calcite, which was in the form of single euhedral crystals. The faster net

468 dissolution of aragonite (i.e., due to increased surface area) would lead to locally higher carbonate
469 concentrations and thus higher (local) saturation indices of cerussite on aragonite than on calcite (Fig. 3A
470 and B; Fig. 4A).

471 Since aragonite and cerussite are isostructural (orthorhombic; 2/m2/m2/m), the isomorphism may be
472 an important factor in determining the reactivity of aragonite to Pb^{2+} relative to calcite. In
473 calcite/aragonite aggregates, rod-shaped crystals of aragonite suggest the preferential growth of aragonite
474 along the c-axis (Wang and Han, 2014; Zeng et al., 2018). Under the reaction conditions of this study,
475 cerussite replacing these aragonite crystals grew dominantly along the c-axis of aragonite (Fig. 4). That is,
476 this observed morphological evolution suggests that the aragonite substrate exerted some control over the
477 cerussite growth. This behavior of cerussite grown on dissolving aragonite is possible due to similar
478 crystal habits of the precipitate and the substrate phases that have the same crystal structures. This
479 crystallographic relationship between aragonite and cerussite may be a cause for the preferential growth
480 of cerussite on aragonite over calcite when these polymorphs coexist. Similar to the relative reactivities
481 observed here, Gamsjäger et al. (1984) observed that Pb^{2+} uptake by aragonite occurred to a greater extent
482 and at a faster rate than that by calcite. On the other hand, Di Lorenzo et al. (2019) reported a lower
483 reactivity of aragonite to Pb^{2+} than calcite and suggested that the surface passivation of aragonite by
484 cerussite may occur due to the isomorphism. We expect that the differences between their and our studies
485 originate from sensitivity to the different experimental conditions. For example, Di Lorenzo et al. (2019)
486 conducted reaction of $CaCO_3$ materials with Pb^{2+} with larger aragonite particles (66 to 250 μm), at less
487 acidic initial pH (= 4.3), and with longer reaction times (4 hr to 10 d) than this study, which induced thin
488 (typically, < 5μm) layers of cerussite on aragonite grains. Overall, the relative reactivities of calcite and
489 aragonite to Pb^{2+} can vary depending on morphological and crystallographic properties of $CaCO_3$
490 materials as well as solution chemistry.

491 Our imaging data provide direct observations of the morphological relationship between the host
492 phases and the secondary minerals upon interaction of $CaCO_3$ minerals with dissolved Cd^{2+} (Figs. 2 to 4).

For all three $CaCO_3$ polymorphs, replacement of aragonite by otavite in acidic Cd^{2+}-containing solutions occurred extensively whereas the formation of otavite on calcite was effectively inhibited (Fig. 3). These observations suggest that the dissolution of calcite is much slower than aragonite in the presence of Cd^{2+}, which could be attributed to interfacial processes such as preferential adsorption of Cd^{2+} and epitaxial growth of otavite on the calcite (104) surface as discussed in the previous section. Overall, our results support the concept that aragonite is much more reactive to Cd^{2+} than calcite under acidic conditions (initial pH 2.7 to 4.0 in this study), in good agreement with previous studies examining Cd uptake by calcite and aragonite under less acidic conditions than this study (initial pH between 5 and 7; Miyake et al. (1988); Pérez-Garrido et al. (2007)).

4.3. Comparison to other related systems

The present results reveal that the replacement reactions in carbonate minerals can be controlled by lattice symmetry and epitaxy/strain. The behavior of calcite in Cd-containing solutions was distinct from the other systems in that calcite rhombs remained essentially unchanged in solutions that were undersaturated with respect to calcite. The mechanistic basiss for this behavior could not be distinguished by our SEM and TXM measurements, indicating that any structural changes resulting from these processes were substantially smaller than the spatial resolution of these imaging techniques (e.g., ~50 nm for TXM). One possible explanation for the inhibition of a replacement reaction is a decreased dissolution of calcite by passivation of their reactive sites. Cd sorption can occur preferentially on the step and kink sites of the calcite surfaces, significantly decreasing surface dissolution rates. Previous AFM observations of the changes in the dissolution pattern of calcite in the presence of Cd corroborate this interpretation (Hay et al., 2003; Pérez-Garrido et al., 2007).

It is also possible that the decreased surface reactivity was due to the formation of a thin epitaxial otavite film that would have the effect of passivating the calcite surfaces. It is known that otavite films can grow from supersaturated solutions that have contained CO_3^{2-} (Callagon et al., 2017; La Plante et al.,

2018). In our case, the growth of otavite relied upon CO_3^{2-} derived from the dissolution of the substrate (Eq. 1), which could be limited if its surface was coated by conformal otavite films. While the detailed properties of these layers were not directly probed here (and will be the subject of subsequent ongoing studies), this hypothesis is not without precedent. For example, the epitaxial growth of otavite and rhodochrosite ($MnCO_3$) on calcite has been demonstrated to passivate the surface reactivity of calcite (Pérez-Garrido et al., 2009; Pérez-Garrido et al., 2007). In a similar vein, observations of dolomite(104) cleavage surfaces in dolomite supersaturated solutions showed the growth of a single epitaxial layer that subsequently passivated the dolomite surface to further growth (Fenter et al., 2007). It was determined that this layer was a Ca-rich $(Ca,Mg)CO_3$ solid-solution layer (presumably due to a higher kinetic lability of the Ca aqua ion than the Mg aqua ion). Because Ca^{2+} is larger than Mg^{2+}, this film would be compressively strained due to the epitaxial constraint with the dolomite substrate, limiting the growth of the film into a thicker layer. This strain-limited growth observed for dolomite is fully consistent with the present observations of inhibited growth in the Cd-calcite system.

It is interesting to compare and contrast the present results to another well-studied system in which epitaxial relationships between the substrate and precipitate might influence the mineral replacement reaction: the replacement of $KBr_{(s)}$ by $K(Cl,Br)_{(s)}$ (Putnis and Mezger, 2004). In the experimental system, solid KBr was in contact with a solution that was saturated with respect to $KCl_{(s)}$ and undersaturated with respect to $KBr_{(s)}$. The dissolution of $KBr_{(s)}$ was observed, coupled with the growth of $K(Cl,Br)_{(s)}$ while retaining the initial crystal shape of the substate. The substrate and the precipitate have the same crystal structure, but with lattice spacing differences as large as ~5% (calculated for the $KCl_{(s)}$ and $KBr_{(s)}$ end members). There are also differences between the K(Cl,Br)/KBr *vs.* the carbonate systems. First, the KBr and $CaCO_3$ replacement reactions occur via exchange between anions and between cations, respectively. The KBr replacement reaction resulted in the formation of $K(Cl_x,Br_{1-x})$ solid solution phases (x is between 0 and 0.5) whose average composition varied depending on the reaction progress (i.e., higher x with an increasing degree of replacement estimated by the film thickness) and evolved from the Br-rich phase

near the K(Cl,Br)/KBr interface toward the Cl-rich phase within the precipitate. In contrast, the $CaCO_3$ reactions involved the formation of either pure (i.e., $PbCO_3$ or $CdCO_3$) or close-to-end-member phases. This difference in composition is explained by analysis of Lippmann diagrams of the K(Cl,Br)/KBr and carbonate systems. Briefly here, the Lippmann diagram consists of solidus and solutus curves, which represent the total solubility product as a function of the solid solution and aqueous solution composition (Lippmann et al., 1980). This diagram is useful to describe the thermodynamic relationship between the solid and aqueous solution phases at equilibrium. The Lippmann diagrams for the two systems reveals much smaller variation in ΔG with x and thus higher compositional variability for the K(Cl,Br) /KBr system than the carbonate systems (Callagon et al., 2017; Putnis and Mezger, 2004). The overall outcome of the KBr reaction would be qualitatively similar to the cerussite/aragonite replacement reaction in which the precipitate grew into the substrate as compared with the otavite/calcite system which appeared self-limiting. The X-ray diffraction data reported by Putnis and Mezger (2004) showed that the K(Cl,Br) layer was orientationally aligned with the KBr substrate. While those results do not directly probe the epitaxial relationships at the K(Cl,Br)-KBr interface at the atomic level, the cross sectional SEM images suggest that there is structural coherence and compositional zoning across the K(Cl,Br)-KBr interface at the nano to microscale level. In addition, the K(Cl,Br) layer had micro-scale cracks, which probably served both as conduits for reactant transport through the precipitate and as a buffer for strain relief within the precipitate layer. These features are similar to our results of the carbonate reactions in which a number of pores were observed within the precipitate layers. Our results from the cerussite/aragonite system also show additional structural gaps at the substrate-precipitate interfaces. Similar structures were not observed in the KBr/KCl study. These detailed comparisons reflect fundamental differences between the K(Cl,Br)/KBr and the carbonate systems associated with the higher compositional flexibility of the K(Cl,Br)-KBr system compared to otavite/calcite and cerussite/aragonite systems.

Conclusions

Systematic comparison among four reaction systems involving replacement of calcite and aragonite by cerussite and otavite enables identification of morphological and crystallographic controls over nano- to micron-scale details of the reactivity of carbonate minerals in acidic metal-containing aqueous solution. In line with our previous studies investigating the internal structures of calcium carbonate polymorphs replaced by cerussite (Kim et al., 2021; Yuan et al., 2016), the present study is the first to provide direct observation on the precipitate-substrate relationship upon aragonite replacement by otavite. Overall, our imaging data indicate that the substrate-precipitate crystallographic relationship can influence the accessibility of fluid to the carbonate substrate and determine spatial extension of coupled dissolution-precipitation processes. The lattice mismatch between the carbonate substrate and precipitate can allow for development of pores at the substrate-precipitate boundaries, as demonstrated by replacement of calcite and aragonite by cerussite and aragonite by otavite. If the lattice match induces the epitaxial growth of the precipitate on the substrate mineral, the lack of porosity at the substrate-precipitate interface can limit further dissolution of the substrate and thus halt the coupled dissolution-precipitation process.

We note that the precipitate-substrate structural relationship examined in this study may depend on the compositional variation in the precipitate. For instance, Xu et al. (2017) demonstrated the formation of epitaxial layers of $(Mn,Ca)CO_3$ solid solution upon calcite reaction with dissolved Mn^{2+}. They concluded that the effective lattice mismatch between the precipitate and the substrate was smaller through Mn-Ca intermixing compared to the nominal lattice mismatch between the two end-members calcite and rhodochrosite ($MnCO_3$) (~10% with respect to the (104) surface). The majority of the previous studies investigating aragonite reaction with Pb^{2+} have pointed out that Pb-dominant carbonate minerals such as cerussite and hydrocerussite are the main products observed on dissolving aragonite. However, the possibility for Pb-Ca intermixing in the product phase cannot be ruled out. Munemoto et al. (2014) suggested that Pb sequestration may occur through two regimes: At relatively low Pb concentration ($[Pb]_{initial}$ = 1-30 μM), Pb was incorporated into the aragonite surface in the form of $(Ca,Pb)CO_3$ solid-

592 solution. Pb-dominant phases such as cerussite and hydrocerussite formed at higher concentrations
593 ($[Pb]_{initial}$ = 50-100 μM). Future research should systematically examine what controls the formation of
594 $(Ca,Pb)CO_3$ solid solution vs. Pb-dominant phases in association with the dissolution of aragonite and
595 whether Ca-Pb intermixing may modify reaction mechanisms during carbonate mineral replacement.

596 The new findings obtained in this study enlarge our current understanding of the reactivity of $CaCO_3$
597 minerals with Pb^{2+} and Cd^{2+} in natural environments. Our results support the concept that the dissolution
598 of calcite and aragonite coupled with the precipitation of heavy metal-containing carbonates is critical for
599 metal sequestration in environments where acidic Pb^{2+}- or Cd^{2+}-contaminated water interacts with
600 carbonate-rich rocks and soils (e.g., acid mine drainage and mine tailings). Because the replacement
601 reactions observed here are relatively fast even under ambient conditions, carbonate minerals present in
602 these carbonate-bearing media are a potential sink for Pb and Cd by transformation to cerussite and
603 otavite.

Acknowledgements

The authors thank Drs. Brandon Fisher and Beihai Ma for help with XRD and Drs. Timothy T. Fister and Rachel E. Koritala for assistance with SEM. We also thank Dalia Delgadillo for assistance in editing and segmenting nano-tomography data. This work was supported by U.S. Department of Energy, Office of Science, Office of Basic Energy Sciences, Chemical Sciences, Geosciences, and Biosciences Division (Geosciences Program) under Contract DE-AC02-06CH11357 to UChicago Argonne, LLC as operator of Argonne National Laboratory. The X-ray data were collected at beamline 32-ID-C, Advanced Photon Source, and we acknowledge the assistance of Drs. Vincent De Andrade and Viktor Nikitin. Use of the Advanced Photon Source was supported by the U.S. Department of Energy, Office of Science, Office of Basic Energy Sciences. The submitted manuscript has been created by UChicago Argonne, LLC, Operator of Argonne National Laboratory ("Argonne"). Argonne, a U.S. Department of Energy Office of Science laboratory, is operated under Contract No. DE-AC02-06CH11357. The U.S. Government retains for itself, and others acting on its behalf, a paid-up nonexclusive, irrevocable worldwide license in said article to reproduce, prepare derivative works, distribute copies to the public, and perform publicly and display publicly, by or on behalf of the Government.

References

Abdilla, B., Minahan, D.J., Gleghorn, J.P., Kim, Y., Lee, S.S., Fenter, P. and Sturchio, N.C. (2022) Emergent Behavior at the Calcite–Water Interface during Reactive Transport in a Simple Microfluidic Channel. ACS Earth Space Chem. 6, 861-870.

Ayachit, U. (2015) The paraview guide: a parallel visualization application. Kitware, Inc.

Busenberg, E., Plummer, L. and Mumpton, F. (1986) A comparative study of the dissolution and crystal growth kinetics of calcite and aragonite. USGS Bull. 1578, 139-168.

Callagon, E., Fenter, P., Nagy, K.L. and Sturchio, N.C. (2014) Incorporation of Pb at the calcite (104)–water interface. Environ. Sci. Technol. 48, 9263-9269.

Callagon, E.B.R., Lee, S.S., Eng, P.J., Laanait, N., Sturchio, N.C., Nagy, K.L. and Fenter, P. (2017) Heteroepitaxial growth of cadmium carbonate at dolomite and calcite surfaces: Mechanisms and rates. Geochim. Cosmochim. Acta 205, 360-380.

Checa, A.G., Jiménez-López, C., Rodríguez-Navarro, A. and Machado, J.P. (2007) Precipitation of aragonite by calcitic bivalves in Mg-enriched marine waters. Mar. Biol. 150, 819-827.

Chiarello, R.P. and Sturchio, N.C. (1994) Epitaxial growth of otavite on calcite observed in situ by synchrotron X-ray scattering. Geochim. Cosmochim. Acta 58, 5633-5638.

Chiarello, R.P., Sturchio, N.C., Grace, J.D., Geissbuhler, P., Sorensen, L.B., Cheng, L. and Xu, S. (1997) Otavite-calcite solid-solution formation at the calcite-water interface studied in situ by synchrotron X-ray scattering. Geochim. Cosmochim. Acta 61, 1467-1474.

Cubillas, P., Köhler, S., Prieto, M., Causserand, C. and Oelkers, E.H. (2005) How do mineral coatings affect dissolution rates? An experimental study of coupled $CaCO_3$ dissolution—$CdCO_3$ precipitation. Geochim. Cosmochim. Acta 69, 5459-5476.

Davis, J.A., Fuller, C.C. and Cook, A.D. (1987) A model for trace metal sorption processes at the calcite surface: Adsorption of Cd^{2+} and subsequent solid solution formation. Geochim. Cosmochim. Acta 51, 1477-1490.

De Carlo, F., Gürsoy, D., Marone, F., Rivers, M., Parkinson, D.Y., Khan, F., Schwarz, N., Vine, D.J., Vogt, S. and Gleber, S.-C. (2014) Scientific data exchange: a schema for HDF5-based storage of raw and analyzed data. J. Synchrotron Radiat. 21, 1224-1230.

Di Lorenzo, F., Ruiz-Agudo, C. and Churakov, S.V. (2019) The key effects of polymorphism during Pb^{II} uptake by calcite and aragonite. CrystEngComm 21, 6145-6155.

Elzinga, E.J., Rouff, A.A. and Reeder, R.J. (2006) The long-term fate of Cu^{2+}, Zn^{2+}, and Pb^{2+} adsorption complexes at the calcite surface: An X-ray absorption spectroscopy study. Geochim. Cosmochim. Acta 70, 2715-2725.

Fedorov, A., Beichel, R., Kalpathy-Cramer, J., Finet, J., Fillion-Robin, J.-C., Pujol, S., Bauer, C., Jennings, D., Fennessy, F. and Sonka, M. (2012) 3D Slicer as an image computing platform for the Quantitative Imaging Network. Magn. Reson. Imaging 30, 1323-1341.

Fenter, P., Zhang, Z., Park, C., Sturchio, N., Hu, X. and Higgins, S. (2007) Structure and reactivity of the dolomite (104)–water interface: New insights into the dolomite problem. Geochim. Cosmochim. Acta 71, 566-579.

Forjanes, P., Astilleros, J.M. and Fernández-Díaz, L. (2020) The formation of barite and celestite through the replacement of gypsum. Minerals 10, 189.

Gamsjäger, H., Fluch, A. and Swinehart, J.H. (1984) The effect of potential aqueous pollutants on the solubility of Pb^{+2} in cerussite—Calcite phase. Monatsh. Chem. 115, 251-259.

Gillikin, D.P., Lorrain, A., Navez, J., Taylor, J.W., André, L., Keppens, E., Baeyens, W. and Dehairs, F. (2005) Strong biological controls on Sr/Ca ratios in aragonitic marine bivalve shells. Geochem. Geophys. Geosyst. 6.

Godelitsas, A., Astilleros, J.M., Hallam, K., Harissopoulos, S. and Putnis, A. (2003) Interaction of calcium carbonates with lead in aqueous solutions. Environ. Sci. Technol. 37, 3351-3360.

Gürsoy, D., De Carlo, F., Xiao, X. and Jacobsen, C. (2014) TomoPy: a framework for the analysis of synchrotron tomographic data. J. Synchrotron Radiat. 21, 1188-1193.

Hay, M.B., Workman, R.K. and Manne, S. (2003) Mechanisms of metal ion sorption on calcite: composition mapping by lateral force microscopy. Langmuir 19, 3727-3740.

Hu, Q., Zhang, J., Teng, H. and Becker, U. (2012) Growth process and crystallographic properties of ammonia-induced vaterite. Am. Mineral. 97, 1437-1445.

Ihli, J., Bots, P., Kulak, A., Benning, L.G. and Meldrum, F.C. (2013) Elucidating Mechanisms of Diffusion- Based Calcium Carbonate Synthesis Leads to Controlled Mesocrystal Formation. Adv. Funct. Mater. 23, 1965-1973.

Kang, C.-H., Han, S.-H., Shin, Y., Oh, S.J. and So, J.-S. (2014) Bioremediation of Cd by microbially induced calcite precipitation. Appl. Biochem. Biotechnol. 172, 2907-2915.

Keith, M., Anderson, G. and Eichler, R. (1964) Carbon and oxygen isotopic composition of mollusk shells from marine and fresh-water environments. Geochim. Cosmochim. Acta 28, 1757-1786.

Kim, Y., Abdilla, B., Yuan, K., De Andrade, V., Sturchio, N.C., Lee, S.S. and Fenter, P. (2021) Replacement of Calcium Carbonate Polymorphs by Cerussite. ACS Earth Space Chem.

La Plante, E.C., Eng, P.J., Lee, S.S., Sturchio, N.C., Nagy, K.L. and Fenter, P. (2018) Evolution of strain in heteroepitaxial cadmium carbonate overgrowths on dolomite. Cryst. Growth Des 18, 2871-2882.

Li, Y.-T., Becquer, T., Dai, J., Quantin, C. and Benedetti, M.F. (2009) Ion activity and distribution of heavy metals in acid mine drainage polluted subtropical soils. Environ. Pollut. 157, 1249-1257.

Lippmann, M., Yeates, D. and Albert, R. (1980) Deposition, retention, and clearance of inhaled particles. Occupational and Environmental Medicine 37, 337-362.

Matthews, J. and Blakeslee, A. (1974) Defects in epitaxial multilayers: I. Misfit dislocations. J. Cryst. Growth 27, 118-125.

Miyake, M., Komarneni, S. and Roy, R. (1988) Immobilization of Pb^{2+}, Cd^{2+}, Sr^{2+} and Ba^{2+} ions using calcite and aragonite. Cem. Concr. Res. 18, 485-490.

Munemoto, T., Fukushi, K., Kanzaki, Y. and Murakami, T. (2014) Redistribution of Pb during transformation of monohydrocalcite to aragonite. Chem. Geol. 387, 133-143.

Pelt, D.M., Gürsoy, D., Palenstijn, W.J., Sijbers, J., De Carlo, F. and Batenburg, K.J. (2016) Integration of TomoPy and the ASTRA toolbox for advanced processing and reconstruction of tomographic synchrotron data. J. Synchrotron Radiat. 23, 842-849.

Perdikouri, C., Piazolo, S., Kasioptas, A., Schmidt, B.C. and Putnis, A. (2013) Hydrothermal replacement of aragonite by calcite: interplay between replacement, fracturing and growth. Eur. J. Mineral. 25, 123-136.

Pérez-Garrido, C., Astilleros, J.M., Fernández-Díaz, L. and Prieto, M. (2009) In situ AFM study of the interaction between calcite {1 0 1^{-} 4} surfaces and supersaturated Mn^{2+}–CO_3^{2-} aqueous solutions. J. Cryst. Growth 311, 4730-4739.

Pérez-Garrido, C., Fernández-Díaz, L., Pina, C.M. and Prieto, M. (2007) In situ AFM observations of the interaction between calcite ($10\bar{1}4$) surfaces and Cd-bearing aqueous solutions. Surf. Sci. 601, 5499-5509.

Plummer, L.N. and Busenberg, E. (1982) The solubilities of calcite, aragonite and vaterite in CO2-H2O solutions between 0 and 90 C, and an evaluation of the aqueous model for the system CaCO3-CO2-H2O. Geochim. Cosmochim. Acta 46, 1011-1040.

Prieto, M., Cubillas, P. and Fernández-Gonzalez, Á. (2003) Uptake of dissolved Cd by biogenic and abiogenic aragonite: a comparison with sorption onto calcite. Geochim. Cosmochim. Acta 67, 3859-3869.

Putnis, A. (2002) Mineral replacement reactions: from macroscopic observations to microscopic mechanisms. Mineral. Mag. 66, 689-708.

Putnis, A. (2009) Mineral replacement reactions, Reviews in mineralogy and geochemistry, pp. 87-124.

Putnis, C.V. and Mezger, K. (2004) A mechanism of mineral replacement: isotope tracing in the model system KCl-KBr-H2O. Geochim. Cosmochim. Acta 68, 2839-2848.

Rai, D., Felmy, A. and Moore, D. (1991) Thermodynamic model for aqueous Cd^{2+}− CO_3^{2-} ionic interactions in high-ionic-strength carbonate solutions, and the solubility product of crystalline CdCO3. J. Solution Chem. 20, 1169-1187.

Riechers, S.L. and Kerisit, S.N. (2018) Anisotropic growth of otavite on calcite: Implications for heteroepitaxial growth mechanisms. Cryst. Growth Des 18, 159-170.

Rouff, A.A., Elzinga, E.J., Reeder, R.J. and Fisher, N.S. (2004) X-ray absorption spectroscopic evidence for the formation of Pb(II) inner-sphere adsorption complexes and precipitates at the calcite− water interface. Environ. Sci. Technol. 38, 1700-1707.

Ruiz-Agudo, C., Álvarez-Lloret, P., Di Lorenzo, F., Gebauer, D. and Putnis, C.V. (2019) Baryte cohesive layers formed on a (010) gypsum surface by a pseudomorphic replacement. Eur. J. Mineral. 31, 289-299.

Ruiz-Agudo, E., Putnis, C. and Putnis, A. (2014) Coupled dissolution and precipitation at mineral–fluid interfaces. Chem. Geol. 383, 132-146.

Sturchio, N.C., Chiarello, R.P., Cheng, L., Lyman, P.F., Bedzyk, M.J., Qian, Y., You, H., Yee, D., Geissbuhler, P. and Sorensen, L.B. (1997) Lead adsorption at the calcite-water interface: Synchrotron X-ray standing wave and X-ray reflectivity studies. Geochim. Cosmochim. Acta 61, 251-263.

Tekawade, A., Liu, Z., Kenesei, P., Bicer, T., De Carlo, F., Kettimuthu, R. and Foster, I. (2021) 3d Autoencoders For Feature Extraction In X-Ray Tomography, 2021 IEEE International Conference on Image Processing (ICIP). IEEE, pp. 3477-3481.

Wang, H. and Han, Y. (2014) A compromise between competing forces dominating the diversity of aragonite structures. CrystEngComm 16, 1971-1977.

Wray, J.L. and Daniels, F. (1957) Precipitation of calcite and aragonite. J. Am. Chem. Soc. 79, 2031-2034.

Xia, F., Brugger, J., Chen, G., Ngothai, Y., O'Neill, B., Putnis, A. and Pring, A. (2009) Mechanism and kinetics of pseudomorphic mineral replacement reactions: A case study of the replacement of pentlandite by violarite. Geochim. Cosmochim. Acta 73, 1945-1969.

Xiong, Y. (2015) Experimental determination of lead carbonate solubility at high ionic strengths: a Pitzer model description. Monatshefte für Chemie-Chemical Monthly 146, 1433-1443.

Xu, M., Kovarik, L., Arey, B.W., Felmy, A.R., Rosso, K.M. and Kerisit, S. (2014) Kinetics and mechanisms of cadmium carbonate heteroepitaxial growth at the calcite ($10\bar{1}$ 4) surface. Geochim. Cosmochim. Acta 134, 221-233.

Xu, M., Riechers, S.L., Ilton, E.S., Du, Y., Kovarik, L., Varga, T., Arey, B.W., Qafoku, O. and Kerisit, S. (2017) Manganese-calcium intermixing facilitates heteroepitaxial growth at the $10\bar{1}$ 4 calcite-water interface. Chem. Geol. 470, 152-163.

Yuan, K., De Andrade, V., Feng, Z., Sturchio, N.C., Lee, S.S. and Fenter, P. (2018) Pb^{2+}–Calcite Interactions under Far-from-Equilibrium Conditions: Formation of Micropyramids and Pseudomorphic Growth of Cerussite. J. Phys. Chem. C 122, 2238-2247.

Yuan, K., Lee, S.S., De Andrade, V., Sturchio, N.C. and Fenter, P. (2016) Replacement of calcite ($CaCO_3$) by cerussite ($PbCO_3$). Environ. Sci. Technol. 50, 12984-12991.

Yuan, K., Starchenko, V., Lee, S.S., De Andrade, V., Gursoy, D., Sturchio, N.C. and Fenter, P. (2019) Mapping three-dimensional dissolution rates of calcite microcrystals: Effects of surface curvature and dissolved metal ions. ACS Earth Space Chem. 3, 833-843.

Zavarin, M., Roberts, S., Hakem, N., Sawvel, A. and Kersting, A. (2005) Eu (III), Sm (III), Np (V), Pu (V), and Pu (IV) Sorption to Calcite. Radiochim. Acta 93, 93-102.

Zeng, M., Kim, Y.-Y., Anduix-Canto, C., Frontera, C., Laundy, D., Kapur, N., Christenson, H.K. and Meldrum, F.C. (2018) Confinement generates single-crystal aragonite rods at room temperature. Proc. Natl. Acad. Sci. 115, 7670-7675.

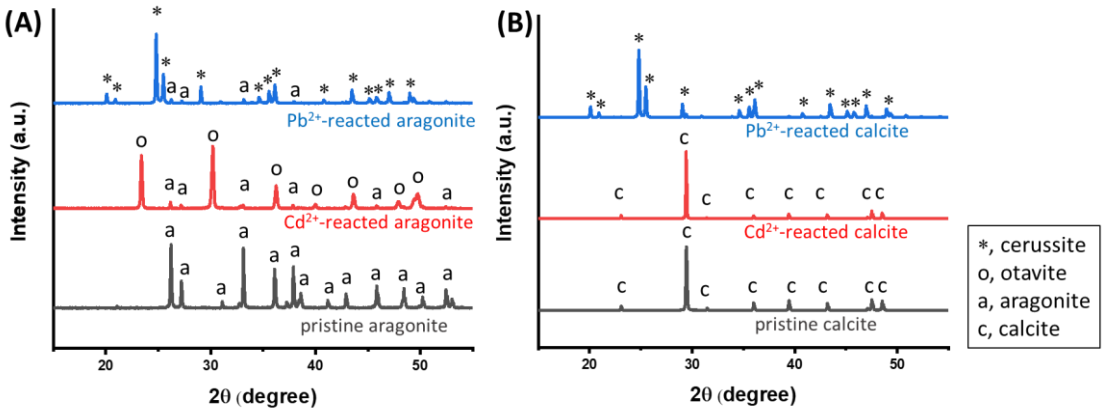

Fig. 1. X-ray diffraction data of (A) aragonite and (B) calcite before (gray) and after reaction with acidic Pb^{2+}- and Cd^{2+}-containing solutions for 16 hr (at pH 2.7; 5 mM $[Pb^{2+}]_{initial}$ (blue) and 5 mM $[Cd^{2+}]_{initial}$ (red), respectively).

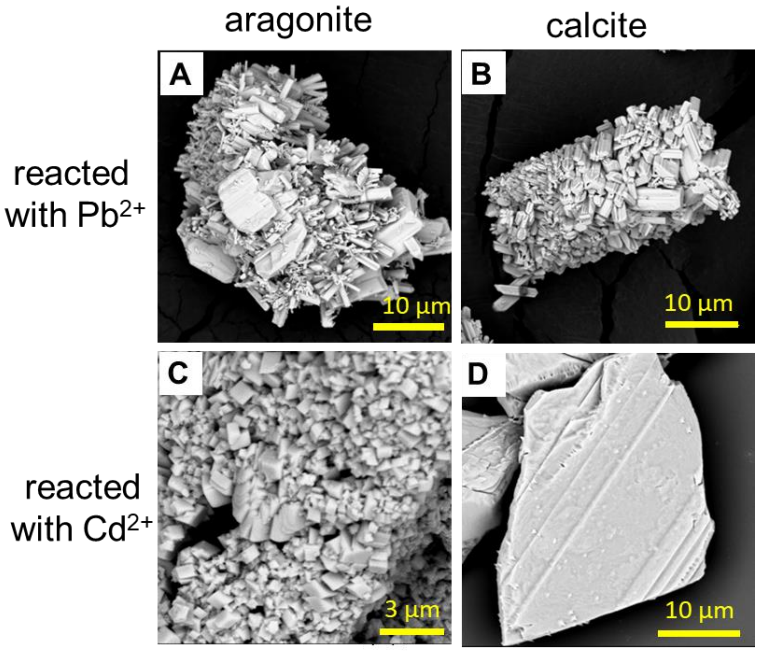

Fig. 2. SEM images of (A, C) aragonite and (B, D) calcite reacted with acidic Pb^{2+}- and Cd^{2+}-containing solutions (at an initial pH 2.7; 5 mM $Pb(NO_3)_2$ and 5 mM $CdCl_2$) for 16 hr. Starting $CaCO_3$ materials were powder specimens of aragonite and calcite. (A, B) Reactions with Pb^{2+} led to rod-shaped cerussite crystals grown on both calcite and aragonite substrates. (C) Aragonite reacted with Cd^{2+} was replaced by rhombohedral otavite crystals whereas (D) no discrete phases of otavite were found for calcite substrates reacted with the Cd solution. The presence of Cd^{2+} on the reacted calcite crystal was detected by EDS (0.03 to 0.11 at.%; Figure S.1) suggesting a sorption reaction.

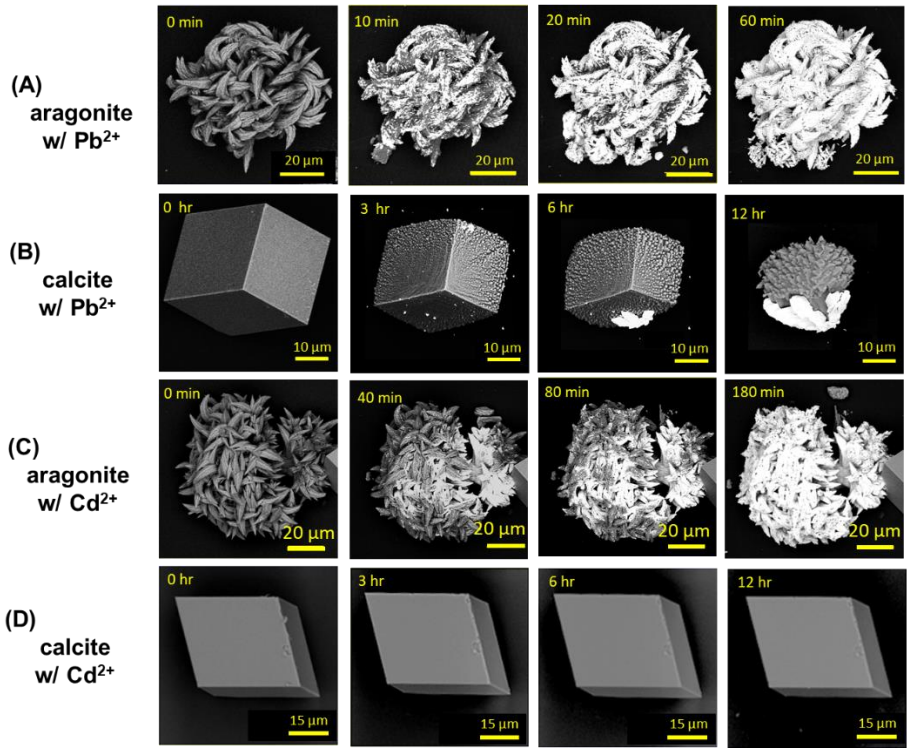

Fig. 3. SEM images of the morphological evolution of individual aragonite and calcite crystals reacted (A, B) in acidic Pb^{2+} solution (initial pH 3.0; 1 mM $Pb(NO_3)_2$) and (C, D) in acidic Cd^{2+} solution (initial pH 4.0; 10 mM $CdCl_2$).

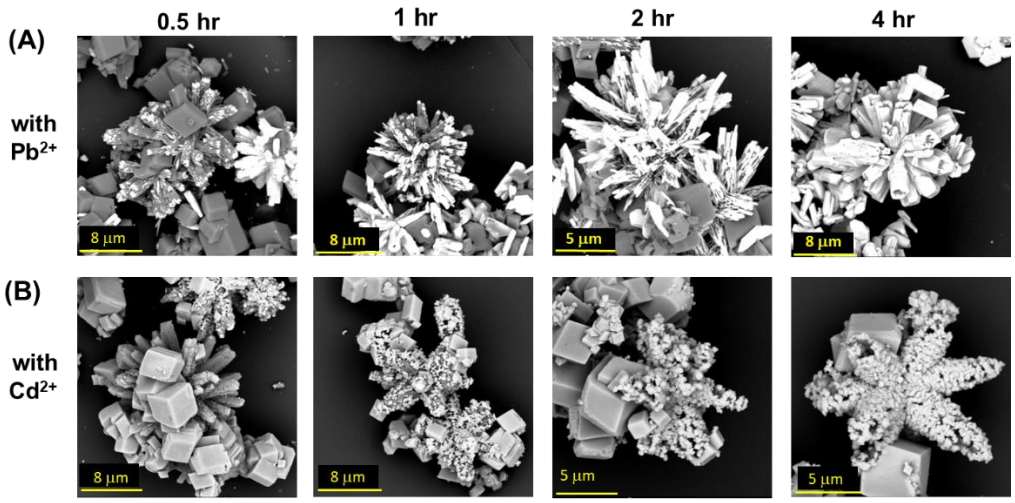

Fig. 4. SEM images of the morphological evolution of calcite/aragonite mixtures reacted with acidic (A) Pb^{2+}- and (B) Cd^{2+}- containing solution (initial pH = 3.0; 5 mM $Pb(NO_3)_2$ and 10 mM $CdCl_2$) for 4 hr.

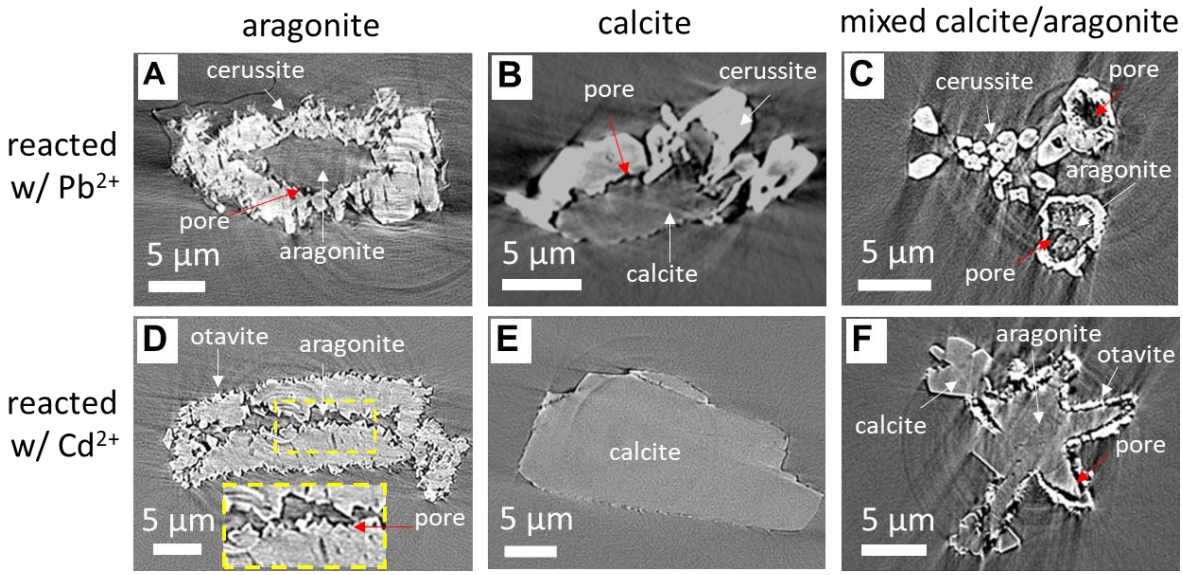

Fig. 5. Nano-tomographic images of (A, D) aragonite and (B, E) calcite powder specimens reacted with acidic Pb^{2+}- and Cd^{2+}- containing solutions (initial pH 2.7; 5 mM $Pb(NO_3)_2$ and 10 mM $CdCl_2$) for 16hr in comparison with (C, F) calcite/aragonite aggregates reacted with acidic Pb^{2+}- and Cd^{2+}-containing solutions (initial pH 3.0; 5 mM $Pb(NO_3)_2$ and 10 mM $CdCl_2$) for 4 hr. (A, B, C, D, F) In Pb^{2+} and Cd^{2+} reacted calcite and aragonite, pores were found between the substrate and the precipitate. (E) In reaction of calcite with Cd^{2+}, the formation of otavite (if any) was limited to the external surface (the thickness of any otavite layer is well-below the resolution of the TXM measurement (50 nm). The internal structure of calcite crystal remains unreacted.

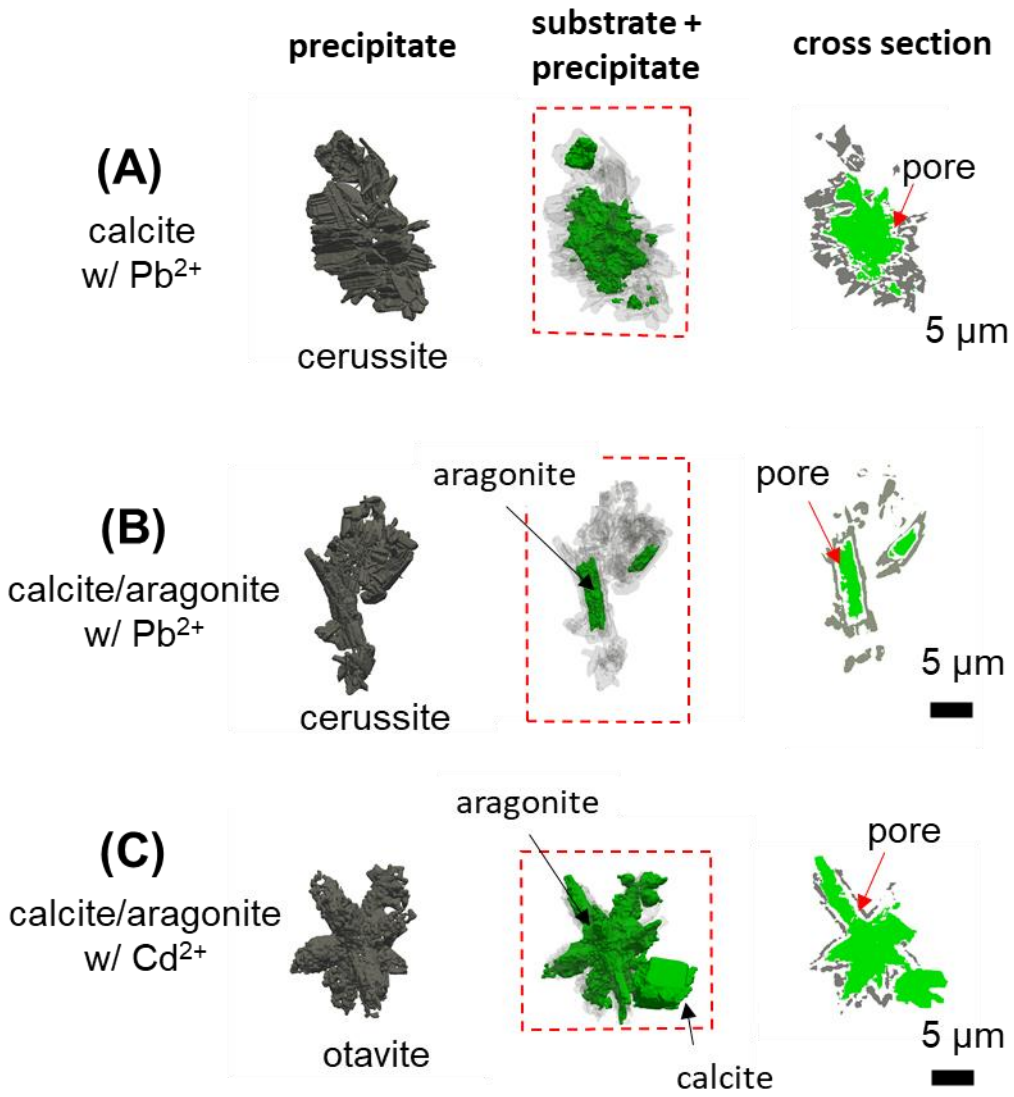

Fig. 6. 3D structures of (A) calcite reacted with Pb^{2+} and (B, C) calcite/aragonite mixture reacted with Pb^{2+} and Cd^{2+}, showing the precipitates, cerussite and otavite, in spatial relationship with the substrate minerals (the first and second columns). The cross sections of these structures (defined in the red-dotted boxes in the second column) are visualized in the third column.